Cell Reports, Volume *31*

Supplemental Information

STING Gain-of-Function Disrupts Lymph Node Organogenesis and Innate Lymphoid Cell Development in Mice

Brock G. Bennion, Carys A. Croft, Teresa L. Ai, Wei Qian, Amber M. Menos, Cathrine A. Miner, Marie-Louis Frémond, Jean-Marc Doisne, Prabhakar S. Andhey, Derek J. Platt, Jennifer K. Bando, Erin R. Wang, Hella Luksch, Thierry J. Molina, Elisha D.O. Roberson, Maxim N. Artyomov, Angela Rösen-Wolff, Marco Colonna, Frédéric Rieux-Laucat, James P. Di Santo, Bénédicte Neven, and Jonathan J. Miner

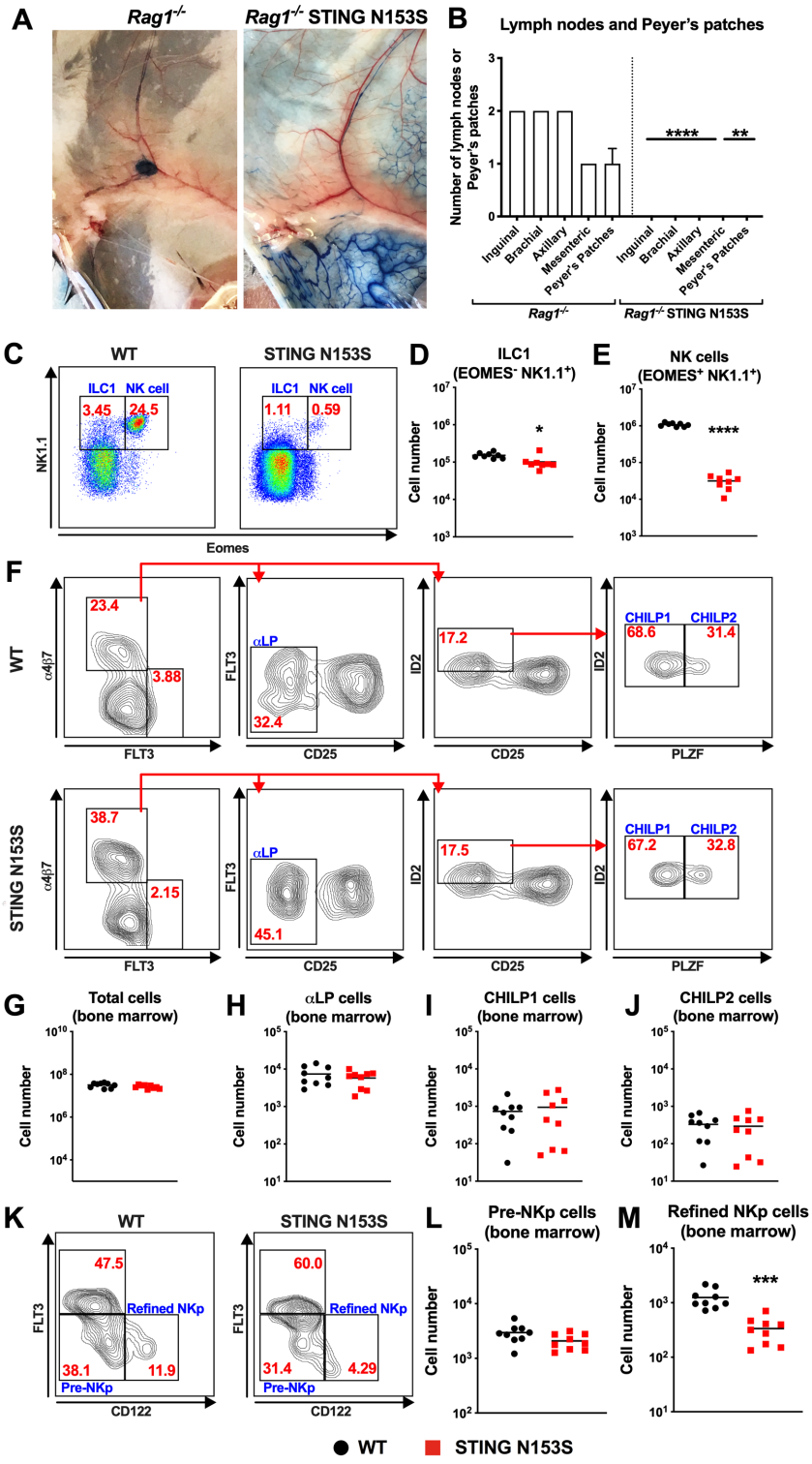

Figure S1. Quantitation of lymph nodes after adoptive transfer and flow cytometric analysis of ILCs in WT and STING N153S animals. Related to Figure 1. (**A**) Representative photographs of *Rag1*$^{-/-}$ (left panel) and *Rag1*$^{-/-}$ STING N153S (right panel) animals following adoptive transfer of WT splenocytes. (**B**) Total number of discernible inguinal, brachial, axillary, and mesenteric lymph nodes and Peyer's patches after adoptive transfer of WT splenocytes. Data represent the mean of 9 mice per genotype. Results were analyzed by Mann-Whitney test. **(C-E)** Flow cytometric analysis on splenocytes from WT and STING N153S littermate mice. (C) Representative FACS plots depicting ILC1 and NK cell populations gated on CD45$^+$CD3$^-$B220$^-$ splenocytes. Total number of ILC1s (D) and NK cells (E) in the spleens of STING N153S and WT mice. Data were collected from 8 mice per genotype. Results were analyzed by unpaired t test. (**F-M**) Bone marrow was collected from adult mice. Representative FACS plots of Lin$^-$CD127$^+$ bone marrow cells (F) from WT (top panels) and STING N153S (bottom panels) littermate mice. Lineage markers for bone marrow ILC progenitor stains include: TER119, B220, CD19, CD11b, CD11c, NK1.1, CD4, CD3ε, CD8α, GR1, Ly6G, and TCRγ/δ. Total number of bone marrow cells recovered (G). Total numbers of αLP cells (Lin$^-$CD127$^+$α4β7$^+$FLT3$^-$CD25$^-$) (H), CHILP1 cells (Lin$^-$CD127$^+$α4β7$^+$FLT3$^-$CD25$^-$ID2$^+$PLZF$^-$) (I), and CHILP2 cells (Lin$^-$CD127$^+$α4β7$^+$FLT3$^-$CD25$^-$ID2$^+$PLZF$^+$) (J). Representative FACS plots (K) of WT (left panel) and STING N153S (right panel) CD3$^-$CD19$^-$NK1.1$^-$CD11b$^-$ CD244$^+$CD27$^+$cKIT^{int}CD127$^+$ cells. Total numbers of Pre-NKp (L) and Refined NKp cells (M). *n* = 9 mice per genotype and data were analyzed by unpaired t test. All data were generated from at least 2 independent experiments. *, $P < 0.05$; **, $P < 0.01$; ***, $P < 0.001$; ****, $P < 0.0001$.

Genotype	Mesenteric	Inguinal	Brachial	Axillary	Number of Peyer's patches/mouse
STING N153S	16%	16%	0%	0%	0.00
Ifnar1$^{-/-}$ STING N153S	0%	0%	0%	0%	0.00
Irf3$^{-/-}$*Irf7*$^{-/-}$ STING N153S	0%	0%	0%	0%	0.00
cGAS$^{-/-}$ STING N153S	20%	0%	0%	0%	0.00
WT	100%	100%	100%	100%	6.83
Ifnar1$^{-/-}$	100%	100%	100%	100%	8.80
Irf3$^{-/-}$*Irf7*$^{-/-}$	100%	100%	100%	100%	8.66
cGAS$^{-/-}$	100%	100%	100%	100%	6.25

Table S1. STING N153S lymph node deficiency in mice lacking downstream effectors of STING, the type I IFN receptor (IFNAR1), and cGAS. Related to Figure 1. STING N153S mice were crossed to *Ifnar1*$^{-/-}$, *Irf3*$^{-/-}$ *Irf7*$^{-/-}$, or *cGas*$^{-/-}$ animals. Adult STING N153S animals deficient for the indicated genes were sacrificed and examined for visual evidence of mesenteric, inguinal, brachial, and axillary lymph nodes and Peyer's patches. Quantitation of the number of discernible lymph nodes compared to littermate controls (e.g., control animals expressing WT STING). Number of Peyer's patches are reported as the mean number observed per mouse. Data were collected from 3-6 mice per genotype in at least 2 independent experiments.

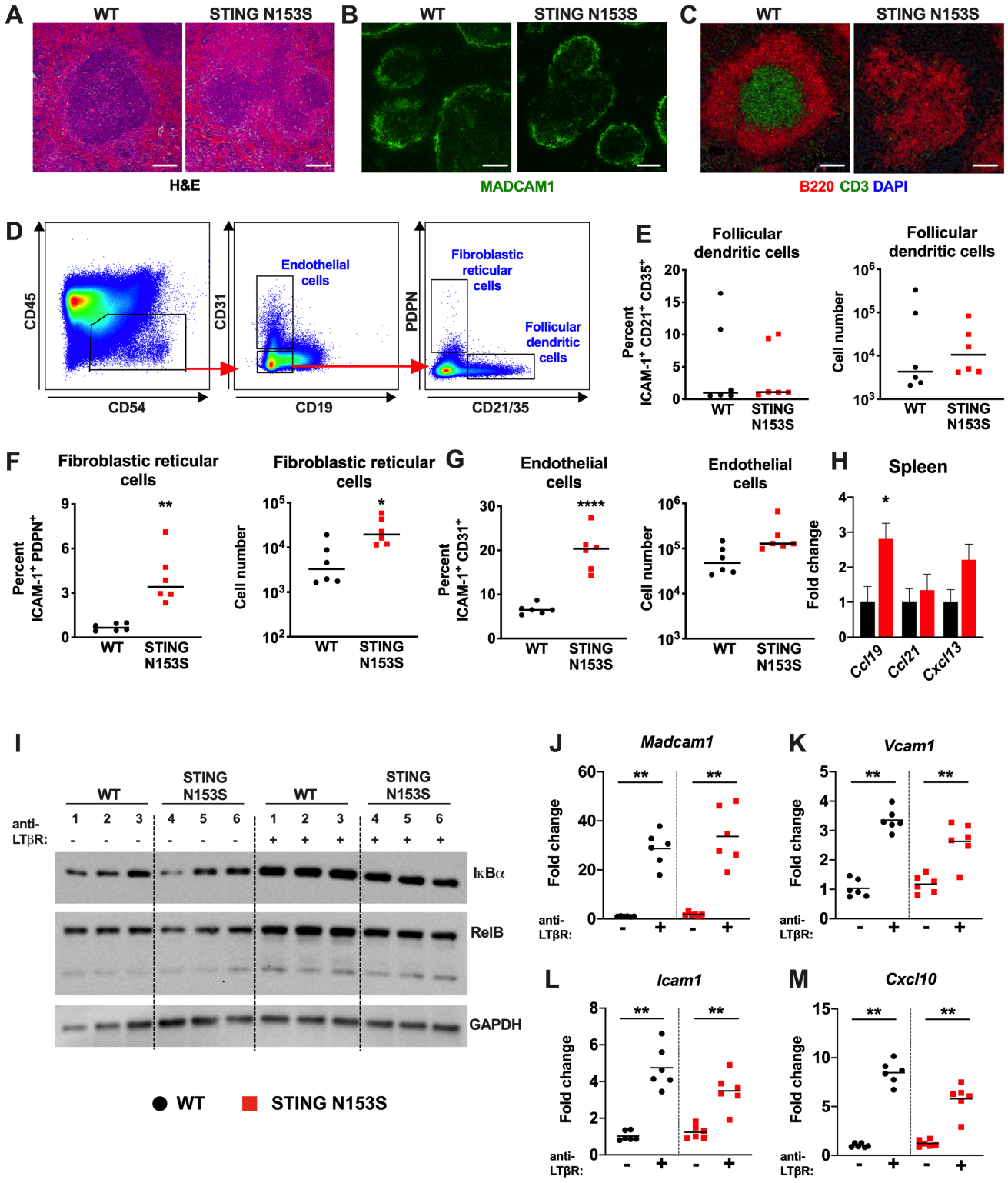

Figure S2. Splenic organization, but not noncanonical NFκB signaling, is perturbed in STING N153S mice. Related to Figure 1. (**A**) H&E staining of paraffin embedded WT (left panel) and STING N153S (right panel) spleen sections. (**B**) MADCAM1 expression (green) in WT (left panel) and STING N153S (right panel) OCT embedded spleen sections (5μm). (**C**) B220 (red) and CD3 (green) expression in WT (left panel) and STING N153S (right panel). Scale bar equals 100 μm. Images are representative of 3 images collected from 3 mice per genotype. (**D**) Gating strategy for splenic stromal cell populations. (**E-G**) FACS quantitation of the percent and number of follicular dendritic cells (E), fibroblastic reticular cells (F) and endothelial cells (G). Data represent the mean of 6 mice per genotype. (**H**) mRNA was isolated from spleen homogenates, and gene expression was quantitated by qRT-PCR for *Ccl19*, *Ccl21*, and *Cxcl13*. Data represent the mean of 8 spleens per genotype. Data in (E-G) were analyzed by unpaired t test and data in (H) were analyzed by Mann-Whitney test. **(I-M)** STING N153S and WT littermate primary MEFs were stimulated with 2 μg/ml anti-LTβR antibody for 24 hours followed by SDS-PAGE, Western blot, or RNA isolation and qRT-PCR analysis. Representative Western blot (I) analysis of IκBα (top panel), RelB (middle panel, top band) and GAPDH from 3 independent generated primary MEF lines per genotype. qRT-PCR analysis of gene expression levels in primary MEFs (J-M). Data represent the mean of 6 samples per genotype and are reported as the fold change relative to control-treated MEFs. All data were pooled from at least 2 independent experiments. Results were analyzed by Mann-Whitney test. *, $P < 0.05$; **, $P < 0.01$; ****, $P < 0.0001$.

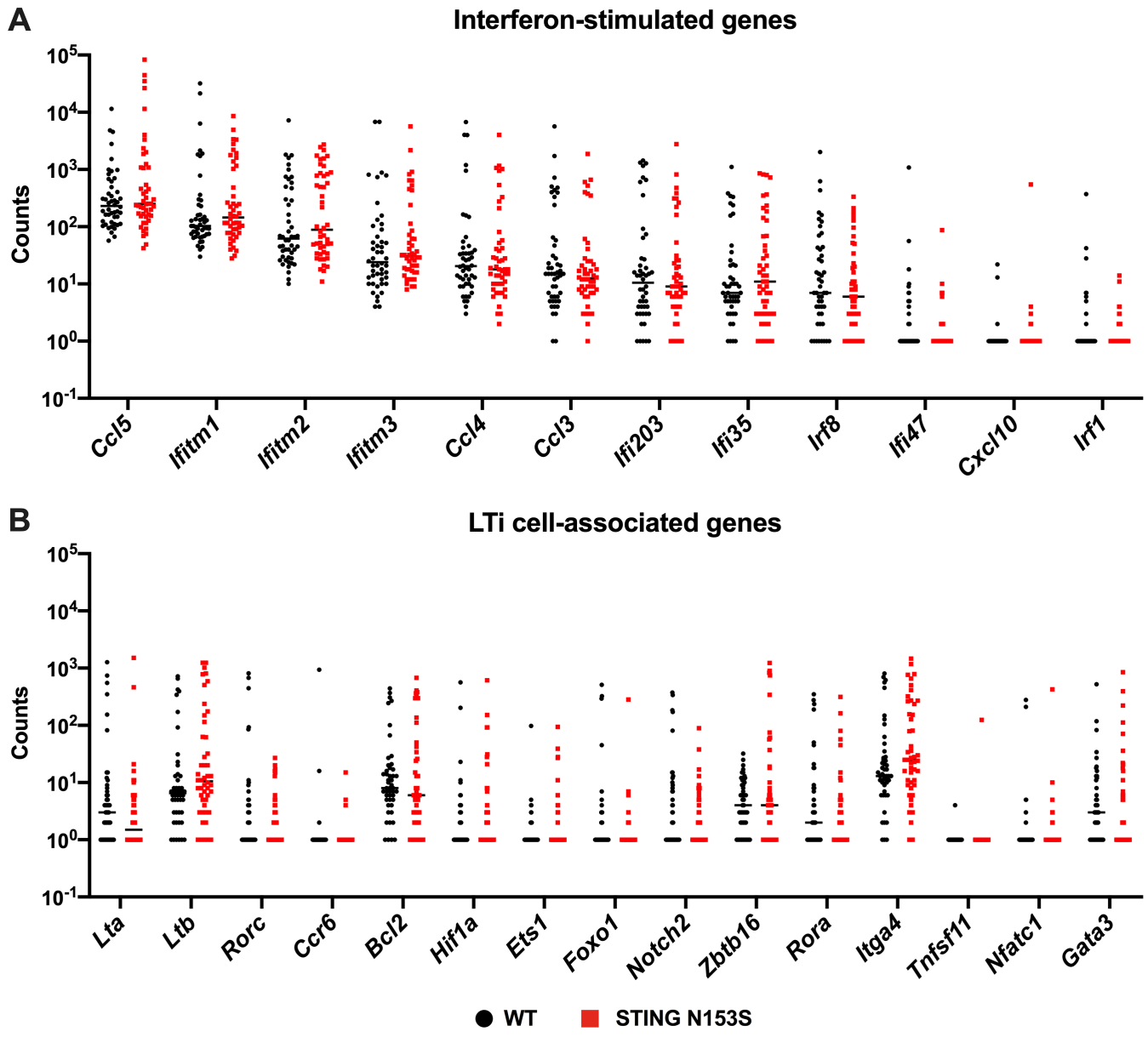

Figure S3. Single-cell RNA-seq analysis of type I IFN-stimulated gene and LTi associated gene expression in WT and STING N153S α4β7⁺ cells. Related to Figure 3. Fetal livers from WT and heterozygous STING N153S animals were harvested on E14.5, and $\alpha4\beta7^+$ cells underwent single-cell FACS sorting into 96-well plates, followed by RNA sequencing. **(A)** Indicated type I IFN-stimulated genes and **(B)** LTi cell-associated genes as measured by FACS-seq analysis of WT and STING N153S $\alpha4\beta7^+$ progenitor cells. Data represent the mean number of counts per gene from 48 cells per genotype performed as a single gene expression screen. Results were analyzed by Mann-Whitney test.

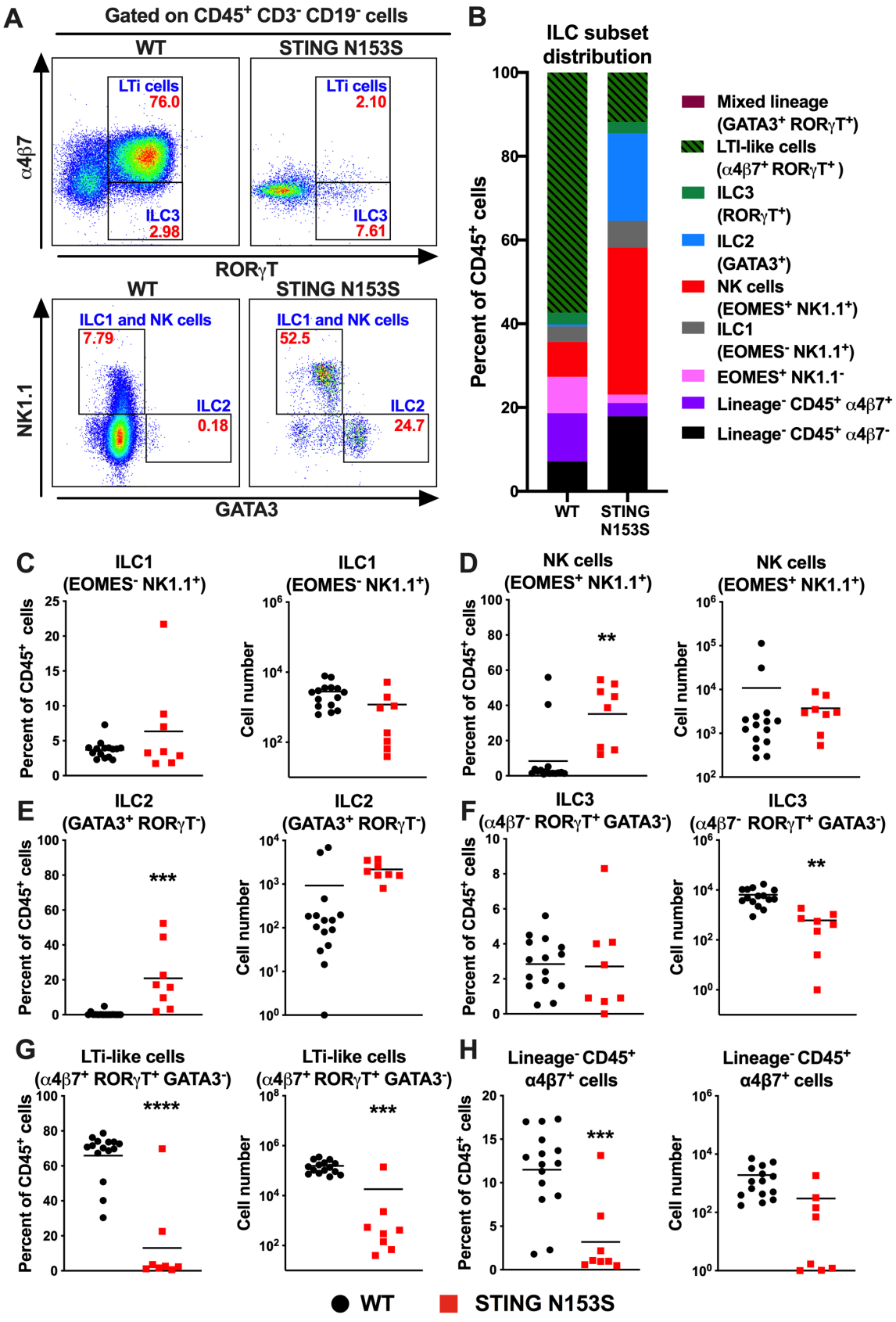

Figure S4. STING N153S fetal liver α4β7$^+$ progenitor cells do not efficiently differentiate into LTi cells after 14 days in an OP9 cell culture system. Related to Figure 4. α4β7$^+$ progenitor cells from the fetal liver were co-cultured with OP9 stromal cells, SCF, and IL-7. Cells were allowed to differentiate for 14-days and analyzed by FACS. (**A**) Representative FACS plots of adult WT (left panels) and STING N153S (right panels) CD45$^+$CD3$^-$CD19$^-$ cells. Cell frequencies within each gate are denoted in red and cell population names are labeled in blue. (**B**) Average frequencies of ILC and α4β7$^+$ cell populations. (**C-H**) Percent and number of ILC1 (C), NK cells (D), ILC2 (E), ILC3 (F), LTi-like cells (G), and Lin$^-$ CD45$^+$ cells (H). Data represent the mean of 8-15 replicates per group pooled from at least 2 independent experiments. Results were analyzed by unpaired t test. **, $P < 0.01$; ***, $P < 0.001$; ****, $P < 0.0001$.

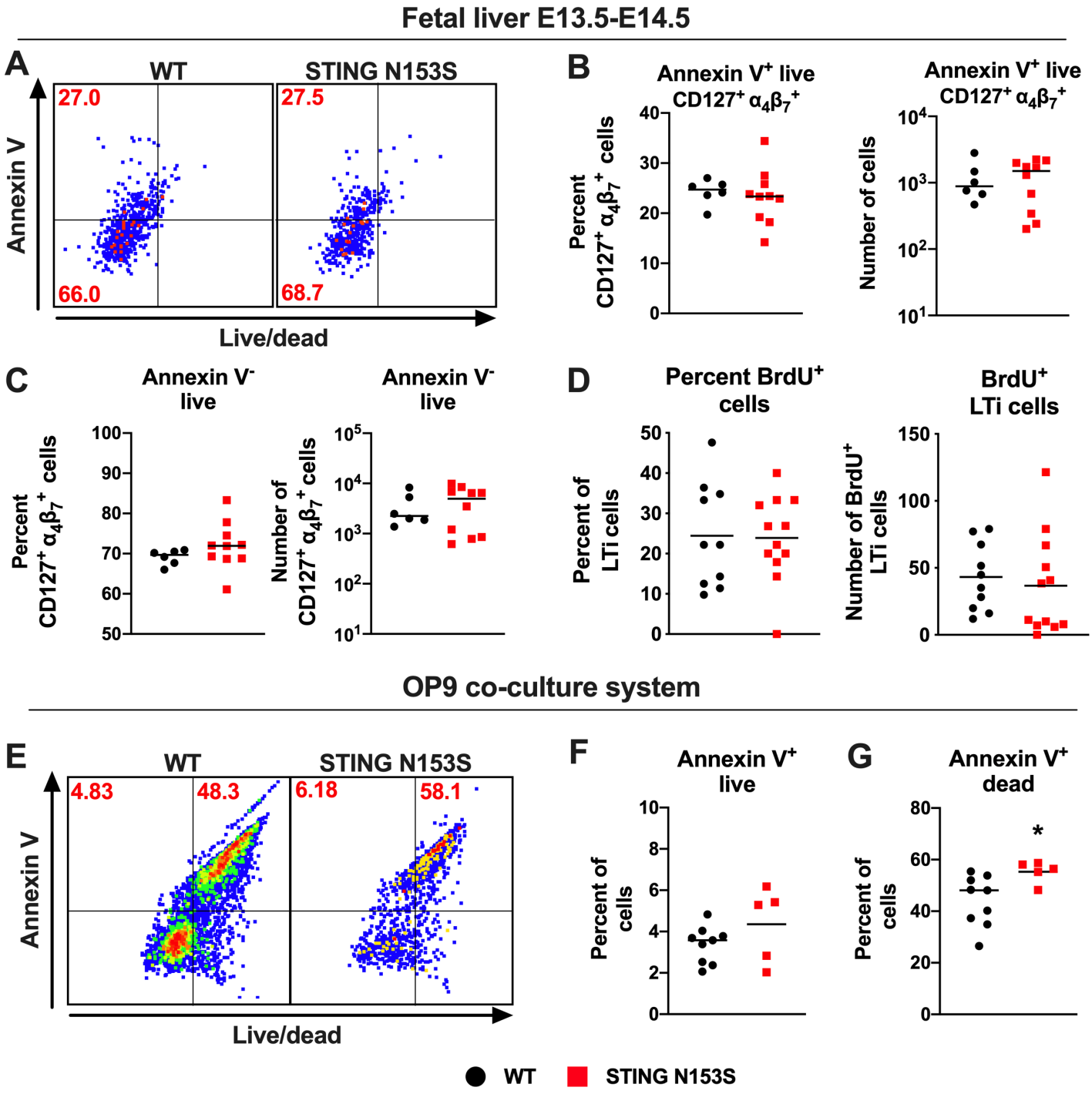

Figure S5. Apoptosis and proliferation in WT and STING N153S LTi and LTi progenitor cells. Related to Figure 4. (**A-D**) Flow cytometric analysis of fetal liver cells from E13.5-E14.5 STING N153S and WT fetuses. Representative dot plots gated on Lin$^-$(CD3, CD5, and CD19) CD45$^+$cKIT^{int}CD127$^+$α4β7$^+$ cells (A). Percent and number of live annexin V$^+$ CD127$^+$α4β7$^+$ cells (B). Percent and number of live annexin V$^-$ CD127$^+$α4β7$^+$ cells (C). Percent and number of BrdU$^+$CD127$^+$α4β7$^+$RORγT$^+$ (LTi) cells (D). Data represent the mean of 6-12 mice per group pooled from at least 2 independent experiments. (**E-G**) α4β7$^+$ progenitor cells from the fetal liver were co-cultured with OP9 stromal cells, SCF, and IL-7. Cells were allowed to differentiate for 6 days and analyzed by FACS. Representative dot plots gated on total cells (E). Percent of annexin V$^+$ live (F) and annexin V$^+$ dead (G) cells from total cells analyzed. Data represent the mean of 5-9 mice per group pooled from 2 independent experiments. Results were analyzed by unpaired t test. *, $P < 0.05$; **, $P < 0.01$; ***, $P < 0.001$.

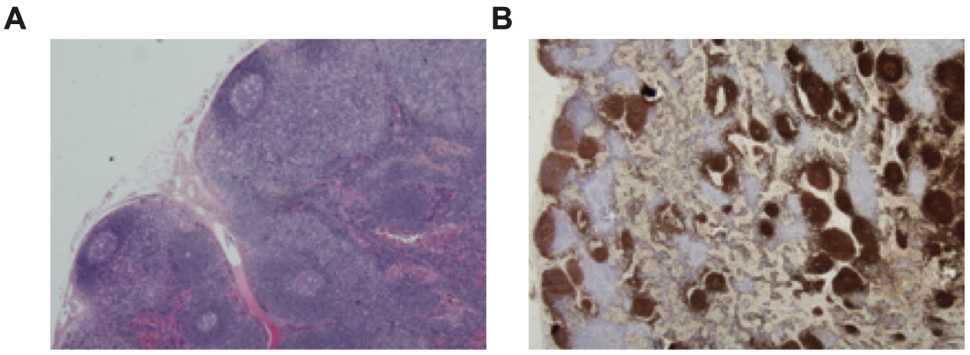

Figure S6. SAVI patient lymph node histology. Related to Figure 5. Representative images of SAVI patient lymph nodes stained with (**A**) hematoxylin & eosin, or (**B**) anti-CD20.

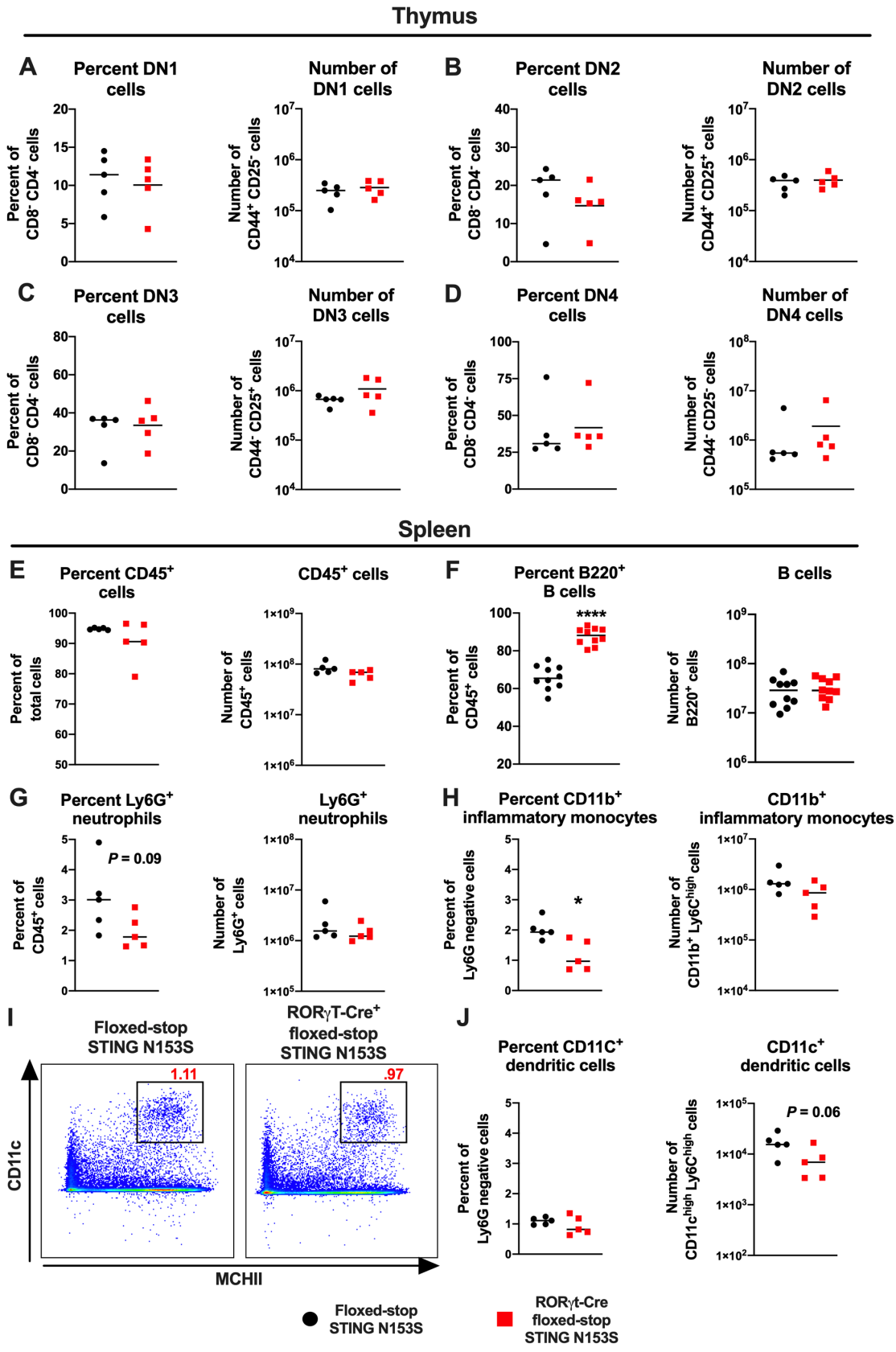

Figure S7. Flow cytometric analysis of double negative T cells in the thymus as well as B cells and myeloid cells in the spleens of RORγT-Cre⁺ floxed-STOP STING N153S mice. Related to Figure 6. (**A-D**) Percent and number of DN1 (A), DN2 (B), DN3 (C), and DN4 cells (D) in the thymus of floxed-STOP STING N153S and RORγT-Cre⁺ floxed-STOP STING N153S mice. Flow cytometric analysis of splenocytes. (**E**) Percent and total number of CD45⁺ cells. (**F-H**) Percent and number of B220⁺ B cells (F), Ly6G⁺ neutrophils (G) and CD11b⁺ inflammatory monocytes (H). (**I**) Representative FACS plots of floxed-STOP STING N153S (left panels) and RORγT-Cre⁺ floxed-STOP STING N153S (right panels) CD45⁺Ly6G⁻ cells. (**J**) Percent and number of CD11c⁺ dendritic cells. Data represent the mean of 5 mice per group pooled from 2 independent experiments. Results were analyzed by unpaired t test. *, $P < 0.05$; ****, $P < 0.0001$.